Submitted to ADVANCED MATERIALS

DOI: 10.1002/adma.000000000

Dual channel operation upon n-channel percolation in a pentacene-C_{60} ambipolar organic thin film transistor

By *Simon J. Noever*, *Stefan Fischer* and *Bert Nickel**

[*] S. Noever, Priv.-Doz. Dr. Bert Nickel
Fakultät für Physik & CeNS
Ludwig-Maximilians-Universität München
Geschwister-Scholl-Platz 1, 80539 Munich (Germany)
E-mail: nickel@lmu.de

Keywords: structure, fullerene, AFM, grazing incidence, heterojunction

Understanding the physics of organic-organic heterojunctions is essential to optimize state of the art organic electronic devices such as organic solar cells, organic light emitting diodes, and ambipolar thin film transistors (TFTs). Ambipolar, as well as combined unipolar TFTs have been assembled and used by several groups to build elemental circuit elements such as inverters and ring oscillators, while light emitting ambipolar TFTs combine the gate controlling features of a transistor with the light emission of a light emitting diode.[1-10] Unfortunately, the energetic landscape at organic-organic interfaces is complicated due to a wealth of electrostatic phenomena such as charge transfer, dipole generation, and doping, all related to aspects of the molecular structure, e.g. molecular orientation, crystallinity, interdiffusion, and domain size. In-situ spectroscopy and diffraction experiments allow for probing the evolution of the electronic and molecular structure of ultrathin organic films during deposition and thus have been fundamental to develop physical models. Such models have been extended and quantified by theoretical studies, leading to a variety of structure dependent mechanisms for heterojunction formation.[11-13] The performance of electronic devices, however, also depends crucially on the balance of several characteristic length scales, i.e. Debye length, depletion width, film thickness, and in particular the spatial location of trap

states. Therefore, it is mandatory to track the evolution of device characteristics with film thickness. The inherent lateral geometry of TFTs allows for the in-situ acquisition of characteristic curves before and during semiconductor deposition. So far, such experiments have focused on hole conducting TFTs. The formation of the conducting channel upon percolation was observed, and from the shift of the threshold voltage with thickness, it was possible to identify surface and bulk traps.[14,15] Here, we expand this technique to ambipolar devices, where the electrostatic situation at the heterojunction is crucial. The basic idea of the experiment is to deposit an electron conducting semiconductor on top of a fully developed p-channel to observe the changes of the device characteristics due to the evolution of an additional n-channel. The in-situ character of this experiment traces electrostatic changes back to the semiconductor layers, rather than external influences like air and humidity, which can significantly alter device characteristics in ex-situ experiments.[16]

We have chosen to study the heterojunction formation of pentacene and fullerene C_{60} because these materials exhibit high charge carrier mobilities in vapor deposited TFTs.[17,18] They have been successfully implemented in various applications, e.g. in organic photovoltaics, and the basic structural and electronic aspects of this heterojunction have already been addresses by atomic force microscopy (AFM), x-ray reflectometry, and photoelectron spectroscopy.[19-26] We complement our in-situ device measurements by grazing incidence x-ray scattering (GIXS) and AFM measurements.

We have tested several contact geometries for the ambipolar device. The best results were obtained employing the device structure depicted in **Fig. 1** (a). The source and drain contacts are located between the two active materials, making the TFT a hybrid structure with a pentacene top contact and a fullerene bottom contact transistor geometry.[5] Hereby, both semiconductors are in direct contact with the electrodes. Note that due to disrupted growth of pentacene on bare Au, top contact geometry is favorable compared to bottom contact. On the other hand, for C60, we have not detected a change of growth topology on the Au contact and

adjacent to it. Thus, we observe that the C60 bottom contact allows for efficient electron injection. Here, Au is used as electrode material, as its workfuction matches the HOMO (highest occupied molecular orbital) of pentacene and the LUMO (lowest unoccupied molecular orbital) of C_{60} reasonably well, offering acceptable injection conditions for holes and electrons into pentacene and C_{60}, respectively.[3] A further advantage of this transistor geometry is an improved C_{60} growth on pentacene with respect to the growth on the gate dielectric.[21,25] We observed the best TFT characteristics with low hysteresis and high mobilities using an SiO_2-Si_3N_4 bilayer as dielectric and a thin cyclic olefin copolymer film of 5 - 6 nm thickness on top. The transconductance characteristics of the ambipolar transistor in ultra high vacuum and at room temperature are shown in Fig. 1 (b). The two curves show the characteristic v-shapes for ambipolar transistors and refer to negative (red curve) and positive (blue curve) source-drain voltages. The minimum current indicates the ambipolar regime of simultaneous electron and hole transport. Previous experiments attribute the observation of this ambipolar regime to the existence of two separate conduction channels; the hole conducting channel is located at the pentacene-gate dielectric interface, whereas the electron conducting channel lies at the pentacene-C_{60} interface.[27] The saturation mobilities of our device calculate to 0.28 $cm^2V^{-1}s^{-1}$ and 0.18 $cm^2V^{-1}s^{-1}$ for holes and electrons, respectively. These values compare to the best performances in ambipolar devices.[3,5] Additionally, the two channels are well balanced in performance, which is a crucial feature for the application in circuits and light emitting TFTs.

To explore the electrostatic changes during the heterojunction formation, we performed C_{60} film thickness dependent measurements, i.e. we recorded gate sweeps for positive source-drain voltages (cf. blue curve in Fig. 1) during fullerene deposition. The resulting transfer curves and their thickness dependence are shown in **Fig. 2** (a). Initially, the transistor shows the expected unipolar hole conducting characteristics of a pentacene based device. During the first 50 Å of deposition, i.e. about 6 ML (monolayers) C_{60}, the characteristic curves hardly

change. Then, at around 55 Å C_{60} film thickness the device suddenly begins to show electron conducting characteristics as well. The thickness resolved values for the respective threshold voltages for hole and electron conduction channel and the electron mobility are plotted in Fig. 2 (b) and (c). Beyond 55 Å, the electron mobility starts to rise quickly with increasing film thickness, until it saturates for thicknesses higher than about 150 Å, i.e. well beyond the Debye length. From unipolar devices it is known that the onset of conduction goes along with percolation of the semiconductor layer.[14] Fast saturation after several pentacene MLs in TFTs has also been described before.[14,28] The threshold voltages here show similar behavior in a sense that no change is measured for the first 50 Å fullerene film thickness. Beyond that thickness, both, the hole and the electron threshold voltages shift oppositely to more positive and more negative values, respectively, i.e. both channels open earlier with respect to their onset voltage. The n-channel threshold voltage experiences a large shift of roughly ΔV_{th} = 7.7 V within 15 Å, i.e. between a nominal fullerene thickness from 55 Å to 70 Å. Thus, the threshold shift occurs within a much narrower thickness range compared to the evolution of mobility.[14] Interestingly, the p-channel threshold mirrors this effect, i.e. it also experiences a shift of about ΔV_{th} = 2.1 V to more positive voltages within fullerene deposition of around 10 Å. This behavior is in agreement with previous observations, where a transistor was measured before and after the deposition of the second semiconductor.[29] In order to verify, whether structural or morphological changes can account for this behavior, we performed complemental structural analysis of the system using AFM and GIXS. The AFM images show that the fullerene film clearly retraces the pyramid like morphology of the underlying pentacene film [**Fig. 3** (a)]. However, it exhibits a drop-like topology with a grain size much smaller than the pentacene grains. This suggests that the delayed conduction onset of the n-channel after around 55 Å (more than 6 ML) is due to percolation of the C_{60} droplets. In addition to morphological studies via AFM we also investigated the crystalline structure of the bilayer. The resulting diffraction pattern [Fig. 3 (b)] shows well known Bragg peaks

stemming from ordered thin film growth of pentacene in [00L] direction.[30-32] This pentacene phase is typical for the employed growth conditions. In addition, this pattern is superimposed by a second set of Bragg features which we have identified to originate from C_{60} face centered cubic (fcc) growth in [111] direction with a lattice constant of a = 14.14 Å. The C_{60} growth corresponds to the well known fcc structure of single crystals at room temperature.[33] The resulting structures are depicted in Fig. 3 (c). Note that reflectometry measurements of C_{60} on pentacene were interpreted as hexagonally closed packed (hcp) C_{60}, one of the known bulk phases of C_{60}. [21,25,34] Here, however, the inplane information of the GIXS measurements allows us to discard hcp stacking and identify fcc as the correct phase for our sample (cf. supporting information). In reflectometry measurements, the fcc [111] direction and the hcp [00L] direction, with L even, are indistinguishable. We are able to index all observed features by considering the identified pentacene and fullerene phase. The absence of additional, not indexed features allows us to exclude a lying down phase of pentacene at the interface or a crystalline interdiffusion layer. Additional off-specular reflectometry x-ray measurements confirm the pentacene thin film growth in [00L] direction and the C_{60} fcc growth in [111] direction and point out high crystallinity of the organic thin films (supporting information). Altogether, the structural information suggests that the C_{60} film follows the underlying pentacene film in a well defined manner without changing its structure.

Consequently, the strong shift of the p-channel threshold voltage has to originate from the electrostatics introduced by the pentacene-C_{60} heterojunction, rather than from structural changes. Highly ordered organic semiconductors exhibit band-like properties such as band dispersion.[26] Additional control of doping levels also allows to tailor the depletion width with respect to the Debye length.[35,36] We assume that pentacene and C60 used here are unintentionally doped semiconductors, as confirmed for pentacene before in double gate experiments.[37-39] In turn, the Fermi levels of pentacene and C60 are expected to align via interface charging, i.e. by formation of depletion zones or accumulation of charges, depending

on the detailed values of the respective Fermi levels. From literature values for the HOMO and LUMO of the two semiconductors we expect the Fermi-level of pentacene to lie above the Fermi-level of C_{60}, i.e. the pentacene side of the interface is to be charged positively, while the C_{60} side is charged negatively.[3] For the pentacene film, this situation resembles a double gate TFT, where a second top channel is accumulated by an additional top gate.[39,40] For simultaneous hole accumulation by the bottom gate, the two hole channels in the pentacene layer do not influence each other due to Debye screening, since the Debye length in pentacene has been found to be a few ML at most.[14] Sweeping the bottom gate voltage to more positive values will at one point switch the pentacene bottom interface from accumulation to depletion, which would lead to a vanishing hole current flow in single gate unipolar TFTs. Here however, the pentacene layer has to be depleted entirely by the bottom gate in order to compensate for the extra top charge at the pentacene-C_{60} interface. Thus, the effective threshold voltage is expected to shift to more positive values, which matches the observed direction of the threshold shift in our device (cf. Fig 2). This confirms the positive precharging of the pentacene top surface and thus the assumption that in pentacene the Fermi-level is closer to the vacuum level than in C_{60}. Furthermore, this experiment is in line with the observation that pentacene double gate transistors are able to form a top channel.[39] The existence of a second conduction channel has also been demonstrated for other ambipolar transistors employing CuPc and F_{16}CuPc.[29]

While the expected n-channel threshold shift is in agreement with the observation, the increasing film thickness, and thus additional volume trap states, also contributes to the shift, as has been found for pentacene based devices before.[14,15]

Remarkably, the shifts of both threshold voltages set in with C_{60} percolation. Obviously, not only the C_{60} n-channel requires percolation, but also the pentacene top channel. The droplet-like growth behavior of C_{60} on pentacene suggests that the heterojunction is confined to the pentacene-C_{60} contact area. At the beginning of fullerene deposition, the Debye length is

much smaller than the lateral distance between C_{60} islands. Thus, before percolation, the inhomogeneous heterojunction landscape resembles a plane of disconnected patches of electrons and holes confined to the interface of the fullerene droplets with the pentacene surface (see **Fig. 4**).[41] The electrostatics and morphology for bottom hole channel accumulation are summarized in the scheme in Fig. 4 (a). The AFM micrograph in Fig. 4 (b) shows early stage C_{60} growth on pentacene and illustrates the disjunct nature of the heterojunction for low fullerene thickness.

As soon as the C_{60} film develops a percolation path between source and drain contact, the heterojunction extends throughout the whole transistor channel length, and the accumulated holes at the pentacene surface can form a percolated top conduction channel. We observe that the threshold shift occurs within only a few Å after percolation, confirming that the heterojunction charging is confined to the interface within the Debye-length.

In summary, we have presented a well balanced ambipolar organic field effect transistor with high hole and electron saturation mobilities of 0.28 $cm^2V^{-1}s^{-1}$ and 0.18 $cm^2V^{-1}s^{-1}$, respectively. The structure and morphology of the respective films have been analyzed using AFM and GIXS methods. Furthermore, we tracked the formation of a pentacene-C_{60} heterojunction by in-situ measurements during deposition of C_{60}. Upon percolation of the n-channel, the heterojunction is charged, acting as an additional top gate for the hole conducting channel. The fact that the p-channel threshold does not shift before the n-channel develops highlights two interesting findings for bilayer ambipolar TFTs. Apparently, before the C_{60} film percolates, the fullerene islands are electronically floating and the charging of the interface is confined to the pentacene-C_{60} contact area. Secondly, the threshold voltage shift of the p-channel upon fullerene percolation implicates the generation of a second hole conducting channel at the pentacene top surface. The introduced method demonstrates a way to evaluate the electrostatic situation in operating organic heterojunction devices. It can be applied to a

variety of vapor depositable organic and inorganic materials and give information about the nature of heterojunctions within other devices such as light emitting diodes and solar cells.

Experimental

Device fabrication and characterization: Highly doped silicon with a bilayer of 100 nm SiO_2 and 100 nm Si_3N_4 was used as the gate contact and dielectric. The surface of the dielectric was cleaned in three steps. First the samples were sonicated in acetone and isopropanol, respectively. After thorough rinsing in DI (deionized) water, the samples were put in Piranha solvent (concentrated sulfuric acid and 30 % hydrogen peroxide solvent at a ratio of 3:1) for 30 minutes. Finally, the samples were plasma cleaned using oxygen plasma (50 W for 30 s, LabAsh). Before depositing the organic materials, a 6 nm thin layer of Topas COC was spin coated onto the silicon nitride surface. We used a 0.25 % COC - toluene solvent at 6000 rpm for 30 seconds. Passivating the surface enhances the growth of pentacene and decrease hysteresis effects in organic thin film transistors. 20 nm of pentacene (triple sublimed, Sigma-Aldrich) were deposited onto the dielectric via molecular beam deposition at a rate of 0.1 $Å s^{-1}$ at room temperature and a chamber pressure of ~ $9 \cdot 10^{-8}$ mbar (as monitored by ion pump current). The 50 nm thick gold source and drain contacts were deposited via electron beam evaporation on top of the pentacene layer. The channel length of 50 µm and the channel width of 2 mm were defined using shadow masks. The hole conducting device was then electrically contacted for the in-situ measurement. 25 nm of the electron conducting C_{60} (sublimed, Sigma-Aldrich) were deposited onto the transistor at a sample temperature of 70 °C and at a rate of 0.1 $Å s^{-1}$ and a chamber pressure of ~$1 \cdot 10^{-6}$ mbar. The sample temperature was measured using a type K thermocouple. While growing the C_{60} layer, transconductance curves were measured with a Keithley Instruments Source Meter 2612 at a frequency of around 1.25 forth- and back-sweeps per minute. In order to obtain the thickness resolved transistor

characteristics the C_{60} layer thickness was measured simultaneously using quartz crystal micro balances.

The GIXS measurements were taken at the W1 beamline at the HASYLAB at DESY in Hamburg. The synchrotron x-ray beam had a wavelength of 1.181 Å. The fabrication of the corresponding samples is equivalent to the samples for the electronic measurements except that the electrodes were omitted.

The AFM micrograph was taken with a Veeco/Digital Instruments NanoScope AFM of the Kotthaus nanophysics group clean room and analyzed with the Nanotec WSxM software [42]. Sketches were made with Adobe Illustrator, the graphs were plotted with OriginLab Origin.

Acknowledgements

The authors gratefully acknowledge financial support from the Deutsche Forschungsgemeinschaft (Grant No. DFG Ni 632-4-1) and the Nanosystems Initiative Munich (NIM). Furthermore, financial support by the Bavarian Ministry for Science through the initiative "Solar Technologies Go Hybrid" (SolTech) is gratefully acknowledged.
We want to thank Wolfgang Caliebe and Ulf Brüggmann for support at the W1 beamline at DESY and we appreciate Matthias Fiebig's contribution towards the thickness resolved measurements.

Received: ((will be filled in by the editorial staff))
Revised: ((will be filled in by the editorial staff))
Published online: ((will be filled in by the editorial staff))

_[1] H. Klauk, U. Zschieschang, J. Pflaum, M. Halik, *Nature* **2007**, *445*, 745-748.

_[2] F. S. Kim, X. Guo, M. D. Watson, S. A. Jenekhe, *Adv. Mater.* **2010**, *22*, 478-482.

_[3] S. D. Wang, K. Kanai, Y. Ouchi, K. Seki, *Organic Electronics* **2006**, *7*, 457-464.

_[4] H. Yan, T. Kagata, H. Okuzaki, *Appl. Phys. Lett.* **2009**, *94*, 023305.

_[5] E. Kuwahara, H. Kusai, T. Nagano, T. Takayanagi, Y. Kubozono, *Chem. Phys. Lett.* **2005**, *413*, 379-383.

_[6] P. Cosseddu, A. Bonfiglio, I. Salzmann, J. P. Rabe, N. Koch, *Organic Electronics* **2008**, *9*, 191-197.

_[7] F. Cicoira, C. Santato, *Adv. Funct. Mater.* **2007**, *17*, 3421-3434.

_[8] J. Zaumseil, R. H. Friend, H. Sirringhaus, *Nature Materials* **2006**, *5*, 69-74.

_[9] R. Capelli, S. Toffanin, G. Generali, H. Usta, A. Facchetti, M. Muccini, *Nature Materials*, **2010**, *9*, 496-503.

_[10] M.A. McCarthy, B. Liu, E. P. Donoghue, I. Kravchenko, D. Y. Kim, F. So, A. G. Rinzler, *Science*, **2011**, *332*, 570-573.

_[11] H. Vázquez, W. Gao, F. Flores, A. Kahn, *Phys. Rev. B* **2005**, *71*, 041306(R).

_[12] F. Flores, J. Ortega, H. Vázquez, *Phys. Chem. Chem. Phys.* **2009**, *11*, 8658-8675.

_[13] S. Verlaak, D. Beljonne, D. Cheyns, C. Rolin, M. Linares, F. Castet, J. Cornil, P. Heremans, *Adv. Funct. Mater.* **2009**, *19*, 3809-3814.

_[14] M. Fiebig, D. Beckmeier, B. Nickel, *Appl. Phys. Lett.* **2010**, *96*, 083304.

_[15] C. Ucurum, H. Goebel, F. A. Yildirim, W. Bauhofer, W. Krautschneider, *J. Appl. Phys.* **2008**, *104*, 084501.

_[16] D. Knipp, A. Benor, V. Wagner, T. Muck, *J. Appl. Phys.* **2007**, *10*, 044504.

_[17] D. Braga, G. Horowitz, Adv. Mater. **2009**, *21*, 1473-1486.

_[18] A. Virkar, S. Mannsfeld, J. H. Oh, M.F. Toney, Y. H. Tan, G. Liu, J. C. Scott, R. Miller, Z. Bao, *Adv. Funct. Mater.* **2009**, *19*, 1962-1970.

_[19] J. Yang, T. Nguyen, *Organic Electronics* **2007**, *8*, 566-574.

_[20] A. K. Pandey, J.-M. Nunzi, *Appl. Phys. Lett.* **2006**, *89*, 213506.

_[21] I. Salzmann, S. Duhm, R. Opitz, R. L. Johnson, J. P. Rabe, N. Koch, *J. Appl. Phys.* **2008**, *104*, 114518.

_[22] S. J. Kang, Y. Yi, C. Y. Kim, K. Cho, H. H. Seo, M. Noh, K. Jeong, K.-H. Yoo, C. N. Whang, *Appl. Phys. Lett.* **2005**, *87*, 233502.

_[23] F. Zhu, M. Grobosch, U. Treske, M. Knupfer, L. Huang, S. Ji, S. Yan, *Appl. Phys. Lett.* **2011**, *98*, 203303.

_[24] Y. Tsuruma, A. Al-Mahboob, S. Ikeda, J. T. Sadowski, G. Yoshikawa, Y. Fujikawa, T. Sakurai, K. Saiki, *Adv. Mater.* **2009**, *21*, 4996-5000.

_[25] K. Itaka, M. Yamashiro, J. Yamaguchi, M. Haemori, S. Yaginuma, Y. Matsumoto, M. Kondo, H. Koinuma, *Adv. Mater.* **2006**, *18*, 1713-1716.

_[26] N. Koch, A. Vollmer, I. Salzmann, B. Nickel, H. Weiss, J.P. Rabe1, *Phys. Rev. Lett.* **2006**, *96*, 156803**.**

_[27] C. Rost, D. J. Gundlach, S. Karg, W. Rieß, *J. Appl. Phys.* **2004**, *95*, 10.

_[28] R. Ruiz, A. Papadimitratos, A. C. Mayer, G. G. Malliaras, *Adv. Mater.* **2005**, *17*, 1795-1798.

_[29] J.Wang, H. Wang, X. Yan, H. Huang, D. Yan, *Appl. Phys. Lett.* **2005**, *87*, 093507.

_[30] C. D. Dimitrakopoulos, A. R. Brown, A. Pomp, *J. Appl. Phys* **1996**, *80*, 2501.

_[31] S. Schiefer, M. Huth, A. Dobrinevski, B. Nickel, *J. Am. Chem. Soc.* **2007**, *129*, 10316-10317.

_[32] S. C. B. Mannsfeld, A. Virkar, C. Reese, M. F. Toney, Z. Bao, *Adv. Mater.* **2009**, *21*, 2294–2298.

_[33] P. A. Heiney, J. E. Fischer, A. R. McGhie, W. J. Romanow, M. Denenstein, J. P. McCauley Jr., Amos B. Smith III, D. E. Cox, *Phys.Rev.Lett.* **1991**, *66*, 22.

_[34] J.L. de Boer, S. van Smaalen, V. Patricek, M. Dusek, M. A. Verheijen, G. Meijer, *Chem. Phys. Lett.* **1994**, *219*, 469-472.

_[35] H. Kleemann, B. Lüssem, K. Leo, *J. Appl. Phys.* **2012**, *111*, 123722.

_[36] H. Kleemann, R. Gutierrez, F. Lindner, S. Avdoshenko, P. D. Manrique, B. Lüssem, G. Cuniberti, K. Leo, *Nano Lett.* **2010,** *10*, 4929–4934.

_[37] S. Verlaak, V. Arkhipov, P. Heremans, *Appl. Phys. Lett.* **2002**, *82*, 745-747.

_[38] T. W. Ng, M. F. Lo, Y. C. Zhou, Z. T. Liu, C. S. Lee, O. Kwon, S. T. Lee, *Appl. Phys. Lett.* **2009**, *94*, 193304.

_[39] M. Göllner, G. Glasbrenner, B. Nickel, *Electroanalysis* **2012**, *24*, 214-218.

_[40] M.-J. Spijkman, K. Myny, E. C. P. Smits, P. Heremans, P. W. M. Blom, D. M. de Leeuw, *Adv. Funct. Mater.* **2011**, *23*, 3231-3242.

_[41] H. Haick, M. Ambrico, T. Ligonzo, R. T. Tung, D. Cahen, *J. Am. Chem. Soc.* **2006**, *128*, 6854-6869.

_[42] I. Horcas, R. Fernandez, J.M. Gomez-Rodriguez, J. Colchero, J. Gomez-Herrero, A. M. Baro, *Rev. Sci. Instrum.* **2007**, *78*, 013705.

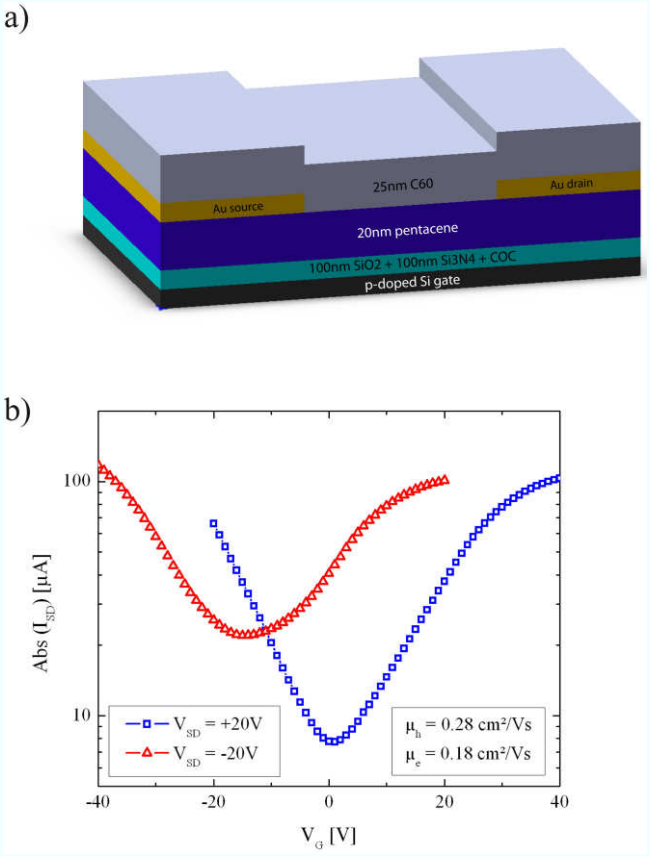

Figure 1. a) Schematic of the ambipolar device structure. b) Transconductance curves of an ambipolar FET for two different source-drain voltages V_{SD}.

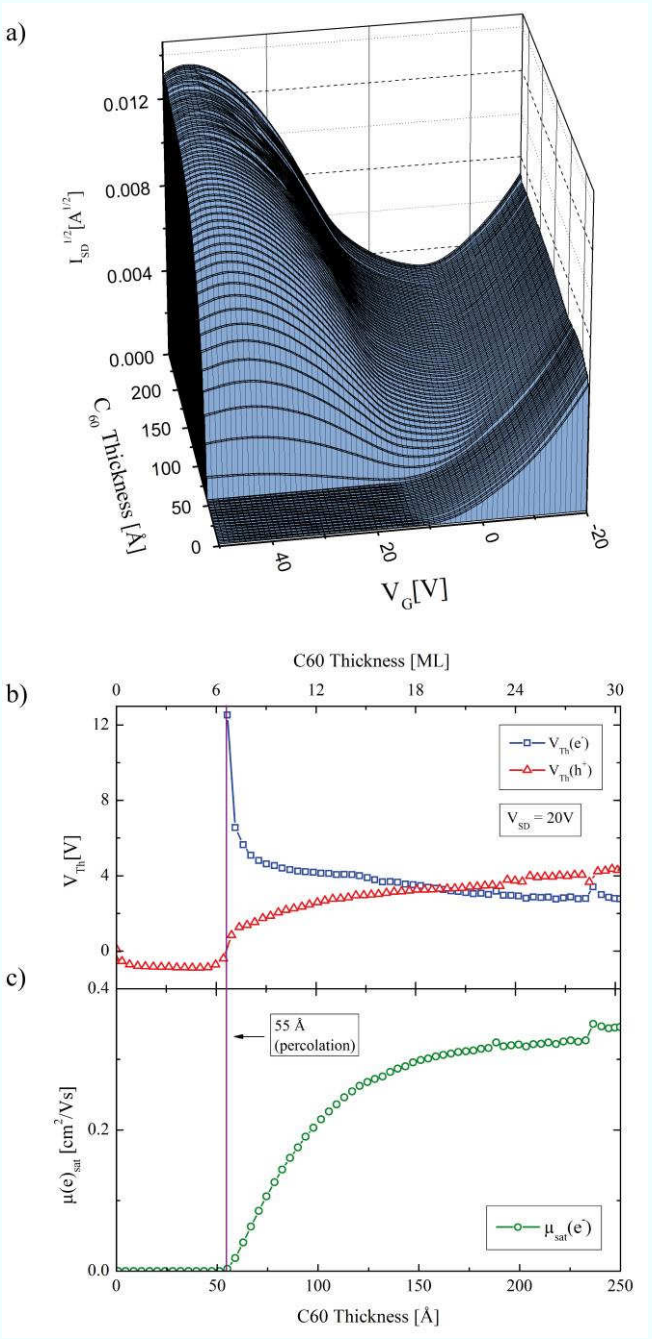

Figure 2. Thickness resolved measurements of the characteristics of an ambipolar FET during C_{60} growth. a) Transconductance curves of an ambipolar TFT as a function of fullerene thickness. b) Thickness resolved threshold voltages of the hole and electron conducting channels, respectively. Percolation of the electron channel is indicated by the vertical line. c) Thickness resolved electron saturation mobility.

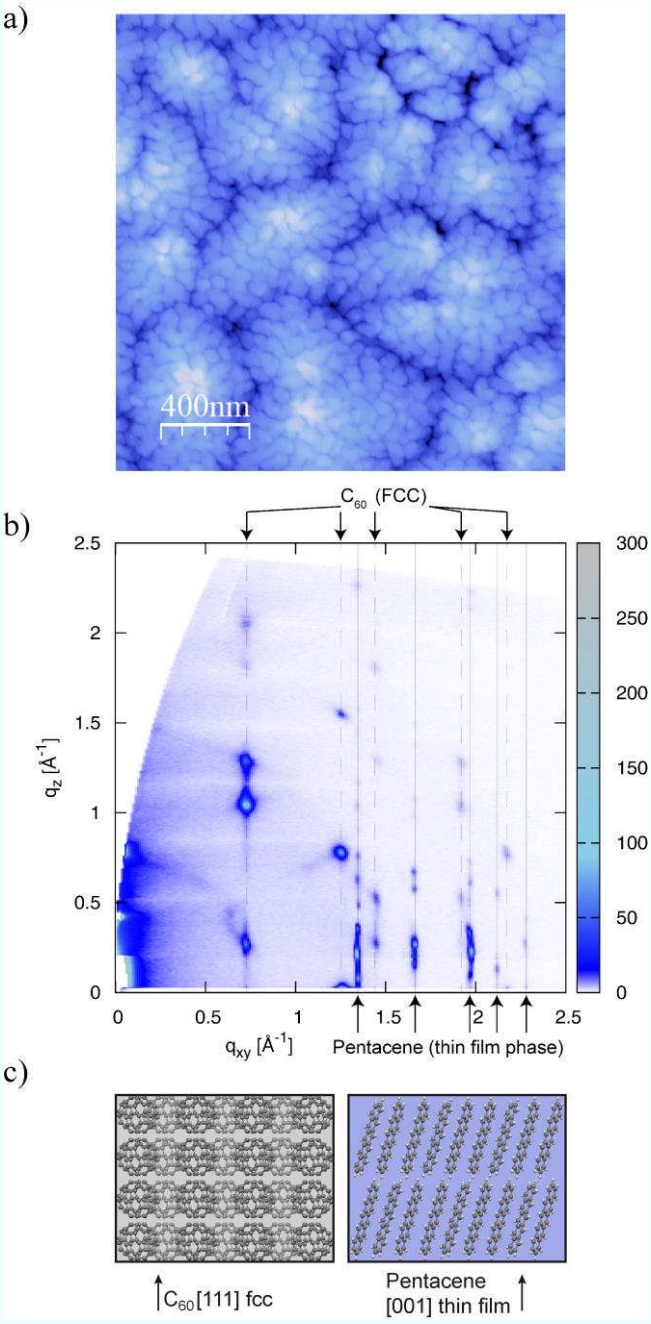

Figure 3. a) AFM height image (2µm x 2µm) of a 25 nm thick C_{60} layer grown on top of a 20 nm thick pentacene thin film layer. b) GIXS measurement of a pentacene-C_{60} bilayer. All diffraction features can be accounted for by a standing up pentacene thin film phase and [111] fcc growth of fullerene C_{60} on top of the pentacene. c) Sketch of fcc [111] direction of crystalline C_{60} and the [00L] thin film phase of pentacene.

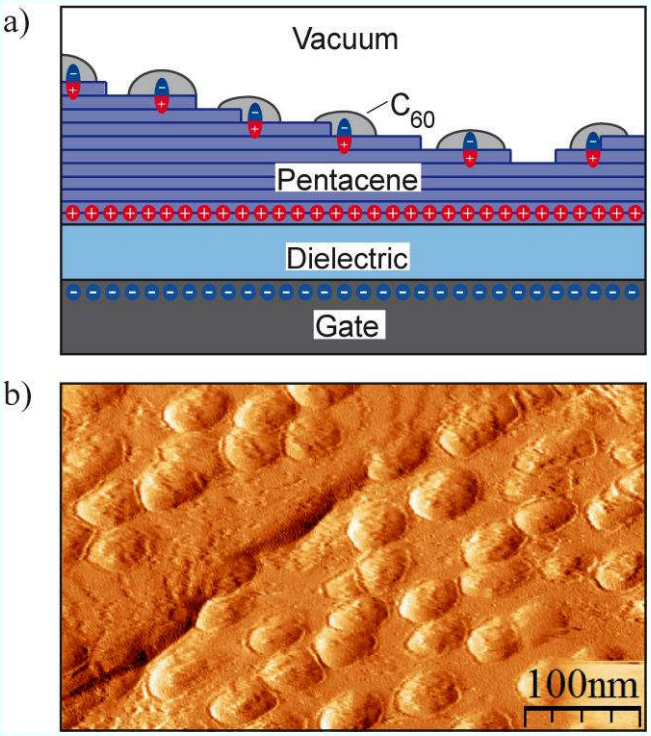

Figure 4. Electronic structure and morphology of the pentacene-C_{60} heterojunction before percolation. a) Scheme of electrostatics in bottom channel hole accumulation (see text). b) Disconnected C_{60} islands (nominal sub-monolayer coverage) on pentacene measured by AFM.

Thickness resolved measurements of ambipolar thin-film transistor characteristics track the charging of an organic-organic heterojunction. Combined with structural investigation methods such as AFM and GIXS, this leads to a better understanding of the physics in state of the art devices such as organic solar cells, organic light emitting diodes and light emitting TFTs.

Keywords: structure, fullerene, AFM, grazing incidence, heterojunction

Simon J. Noever, Stefan Fischer and Bert Nickel*

Dual channel operation upon n-channel percolation in a pentacene-C_{60} ambipolar organic thin film transistor

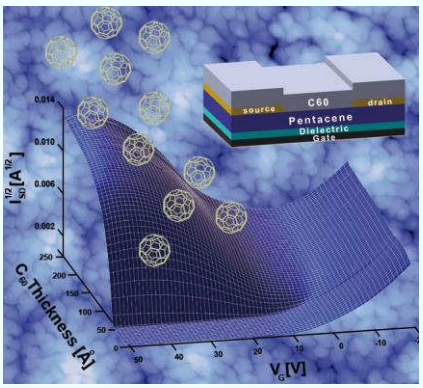

Supporting Information
Supporting Information is available online from Wiley InterScience or from the author.

Submitted to ADVANCED MATERIALS

Supporting information for:

Dual channel operation upon n-channel percolation in a pentacene-C_{60} ambipolar organic thin film transistor

By *Simon J. Noever*, *Stefan Fischer* and *Bert Nickel**

[*] S. Noever, Priv.-Doz. Dr. Bert Nickel
Fakultät für Physik & CeNS
Ludwig-Maximilians-Universität München
Geschwister-Scholl-Platz 1, 80539 Munich (Germany)
E-mail: nickel@lmu.de

GIXS measurement of pentacene-C_{60} heterojunction:

GIXS measurement of the pentacene-C_{60} bilayer with full indexing of all diffraction features. The measurement confirms the standing up pentacene thin film phase and [111] fcc growth of fullerene C_{60}. A sketch of the measurements geometry is depicted below.

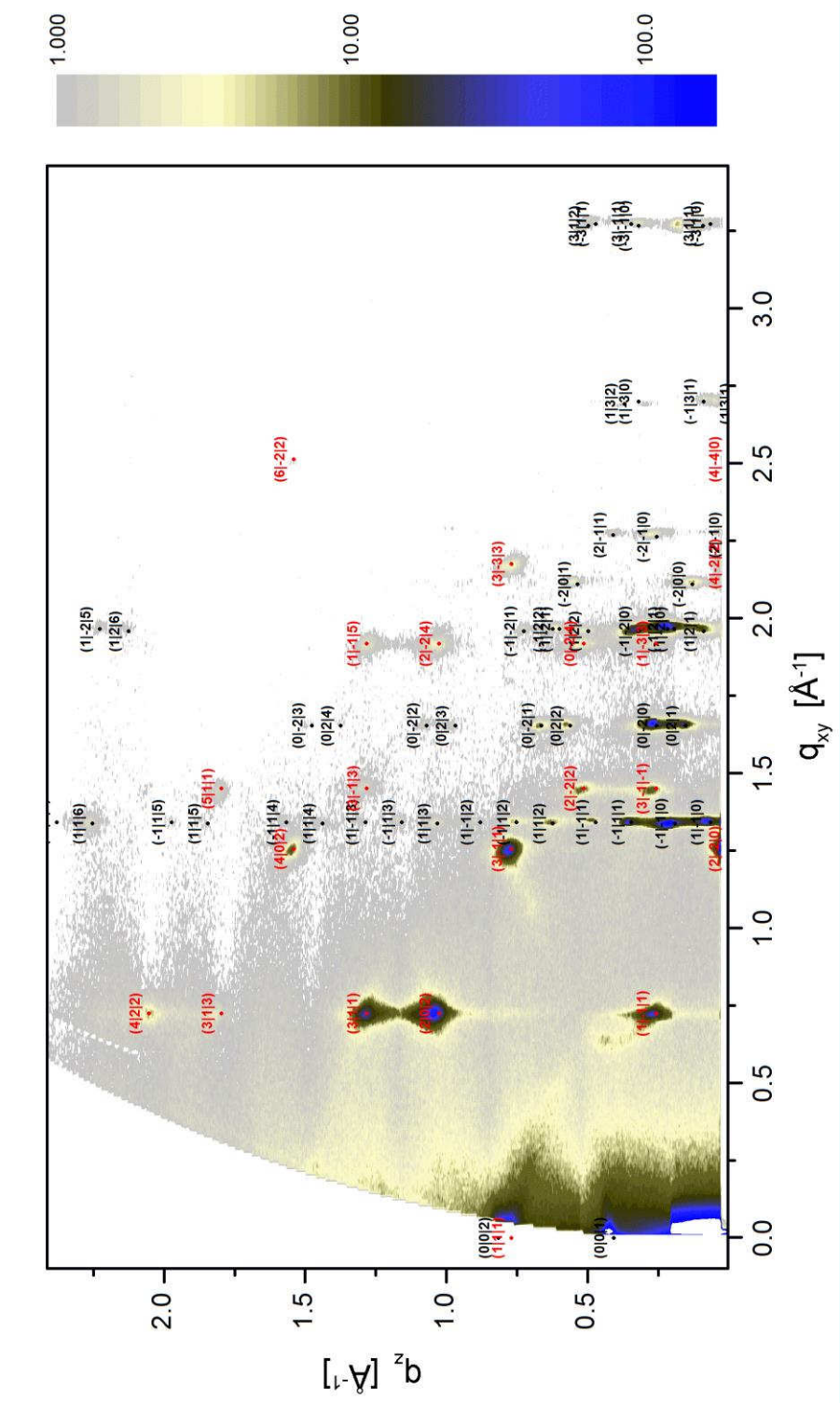

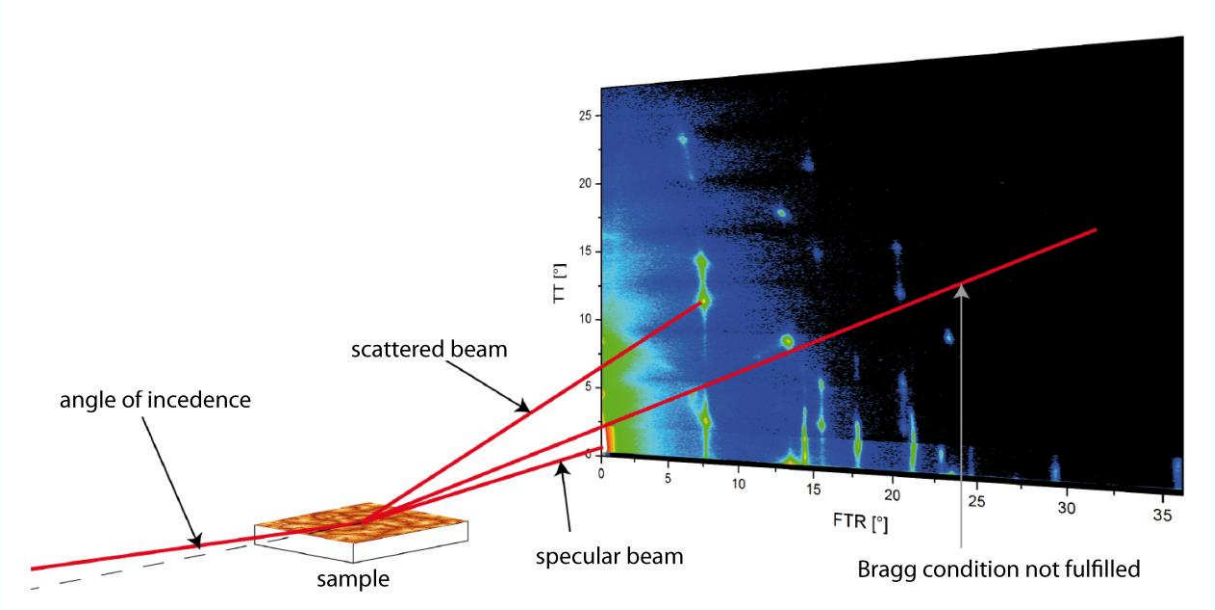

Calculated hcp features of C_{60}:

GIXS measurement of the pentacene-C_{60} bilayer. The indices show the calculated positions for hcp stacking of fullerene C_{60}. Clearly the measured features cannot account for such a crystal structure.

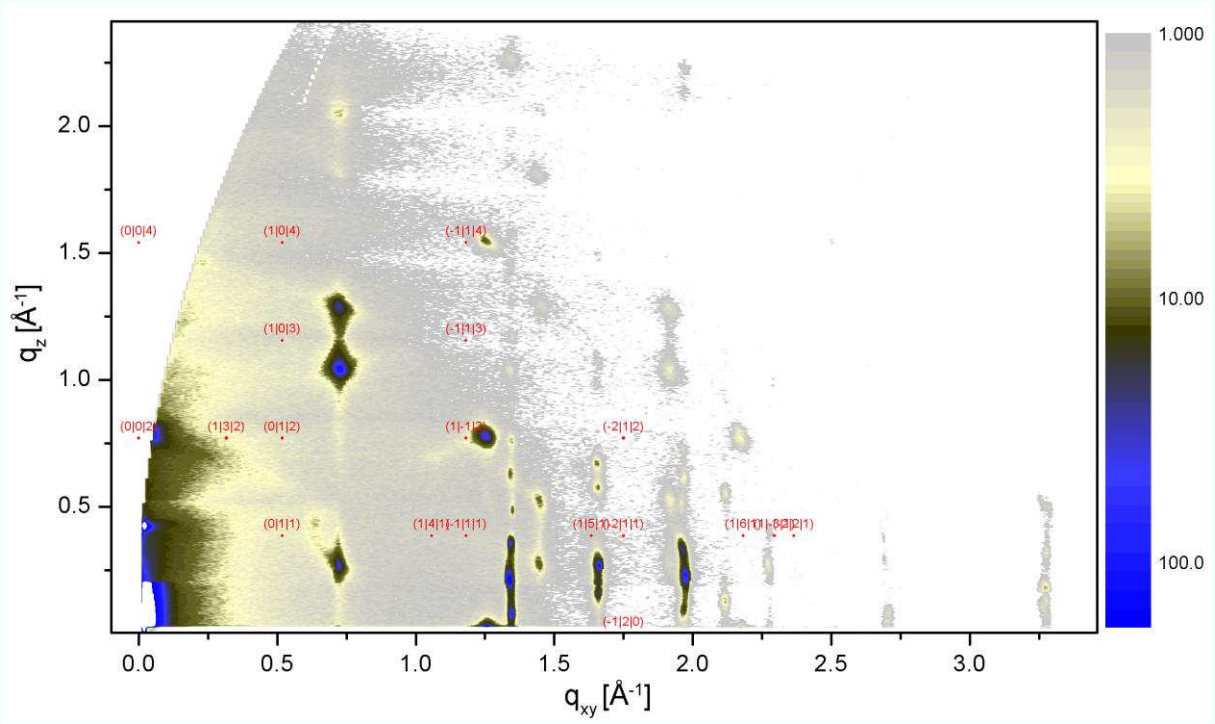

Off-specular x-ray measurement:

The off-specular diffraction pattern of a pentacene-C_{60} bilayer emphasizes the good crystallinity of both semiconductors (notice the scales of the in-plane and the out-of-plane components of the momentum vector q).

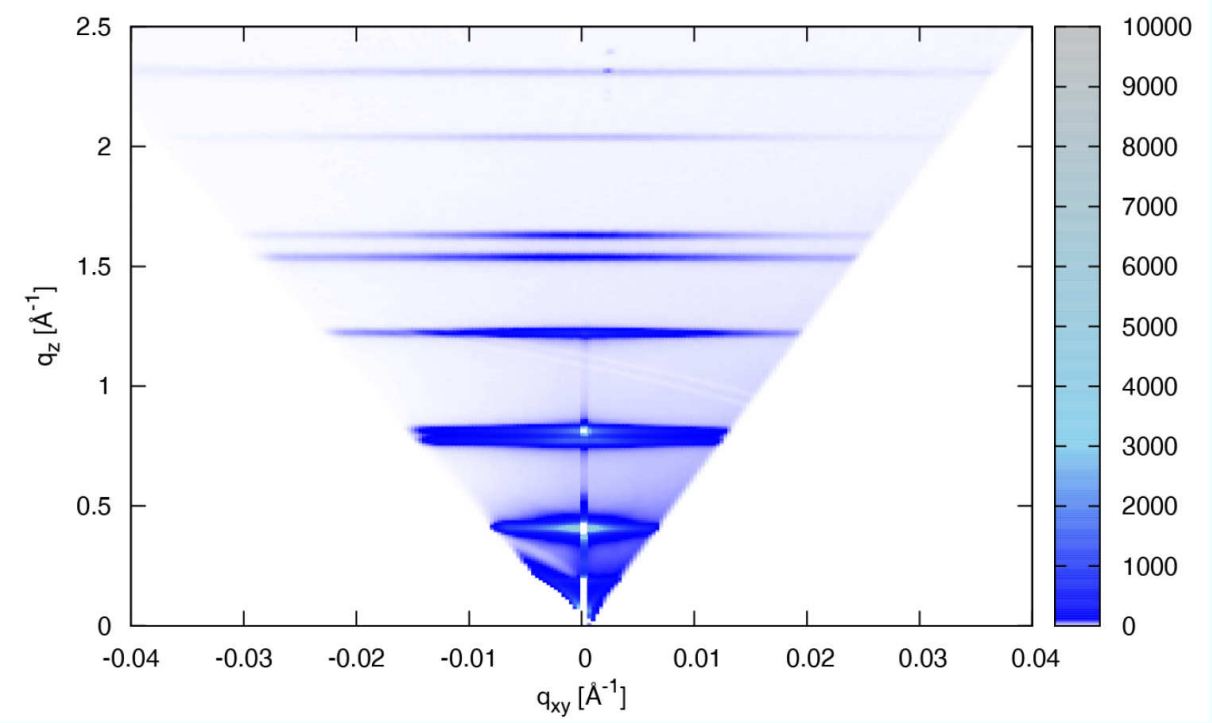

Schematic of the electrostatics of the final device (after fullerene deposition):

At highly negative gate voltages the ambipolar device is in the unipolar hole conducting regime with an accumulation channel at the pentacene-dielectric interface [a)]. The case for unipolar electron conductance is shown in b) where the pentacene contributes to the dielectric and the active channel is located at the pentacene-C_{60} interface. The pentacene-C_{60} interface bias is indicated by a symbolic dipole.

c) shows the direction of the band alignment at the pentacene-fullerene interface. No claim for quantitative accuracy is made for this scheme. It shows however that the expected sign of the interface bias is in agreement with the measured threshold shift. The energy barriers introduced by the discontinuities prevent the charge carriers to recombine.

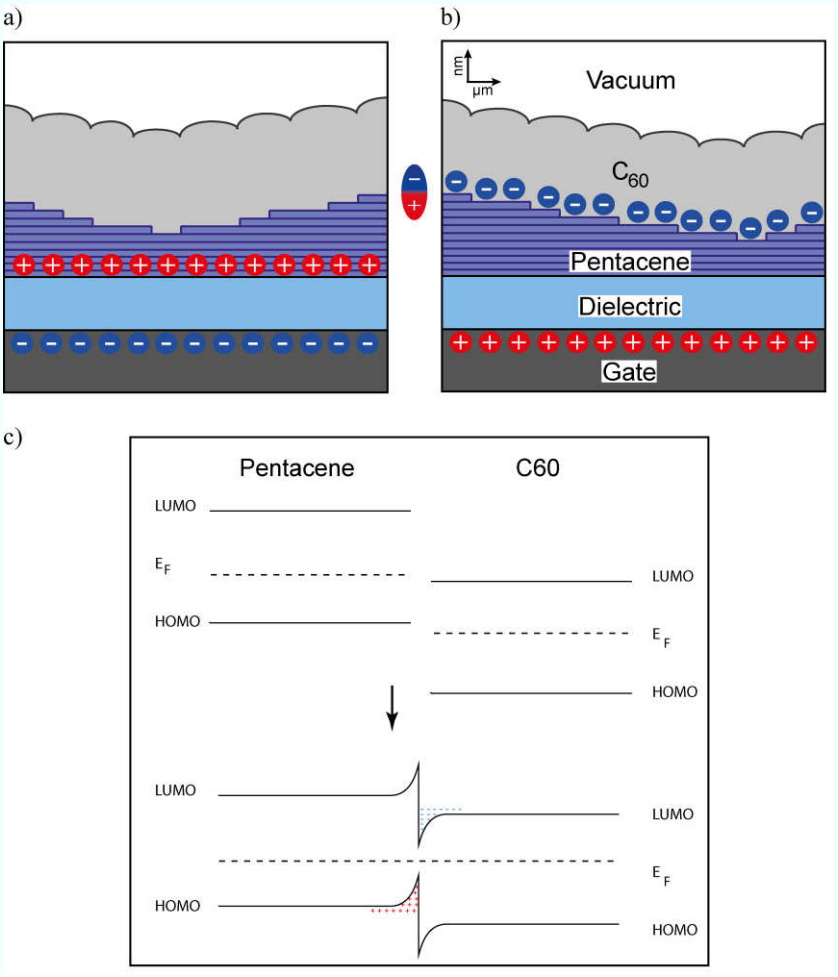

When the device is illuminated directly by a red laser-pointer, strong photo-response is observed. In future experiments, it would be very interesting to investigate also the thickness dependent optoelectronic properties of such heterojunctions in TFT geometry.